A COMPREHENSIVE ANALYSIS OF THE BIOGRAPH VISION PET/CT SYSTEM USING NEMA-2-2012

S. Kheruka, N. Al-Maymani, N. Al-Makhmari, H. Al-Saidi, T. Raii, S. Al-Rashdi, A. Al-Balushi, V. Jayakrishnan, Anjali Jain, K. Al-Riyami, R. Al-Sukaiti

Department of Radiology and Nuclear Medicine, Sultan Qaboos Comprehensive Cancer Care and Research Centre, Muscat, Oman

Abstract— **This study examines the Biograph Vision 600 PET/CT system from Siemens Healthineers. Equipped with silicon photomultiplier-based detectors, this system focuses on enhancing imaging quality. By incorporating SiPM detectors and 3.2 mm LSO crystals, it maximizes scintillator coverage. The system comprises eight rings, each housing 38 detector blocks, which are further divided into 4x2 mini blocks. These mini blocks feature a 5x5 LSO array connected to a 16x16 mm SiPM array. Together, this configuration offers an axial FOV of 26.1 cm. The study evaluates the system's performance against the NEMA NU 2 2012 standard, assessing key metrics like spatial resolution, sensitivity, count rate dynamics, scatter correction efficiency, TOF performance, and overall image quality. Results show a NEMA sensitivity of 15 kcps/MBq, an axial spatial resolution of 3.2 mm (with a 1 cm offset from the FOV center), a peak NECR of 300 kcps at 32 kBq/mL concentration, and a TOF timing resolution of 213 ps. Image quality phantom tests based on NEMA standards indicate contrasts ranging from 77% to 92.5% and 80.8% to 90.9% for sphere-to-background ratios of 4:1 and 8:1, respectively. The Biograph Vision 600 PET/CT system conforms to NEMA standards, showing promise for clinical use and advanced diagnostics.**

Keywords— PET/CT, NEMA.

I. INTRODUCTION

Positron Emission Tomography (PET) is now a vital tool in the medical field, especially for the diagnosis and monitoring of various health conditions. The introduction of the first integrated PET/CT system in 1998 marked a significant advancement in medical imaging techniques [1]. Over time, PET technology has made impressive progress. The incorporation of lutetium oxyorthosilicate crystals has enhanced coincidence timing windows, allowing the development of time-of-flight (TOF) imaging methods [2-5]. Moreover, widening the axial field of view (FOV) has improved the capability to capture volumetric data [6].

The precision and efficiency of PET systems play a critical role in accurate clinical diagnoses. Standards like the NEMA NU 2-2012, set by the National Electrical Manufacturers Association (NEMA), outline comprehensive protocols for evaluating the technical performance of these systems. These standards ensure consistent assessments and provide a reliable foundation for comparing different PET systems [7].

In this dynamic landscape, different digital PET/CT systems have been engineered, including the Biograph Vision 600 by Siemens Healthineers, the Vereos by Philips Healthcare, and the Discovery MI by GE Healthcare [8-10]. These systems feature silicon photomultiplier (SiPM) detectors and lutetium oxyorthosilicate crystals to enable efficient interfacing and enhance imaging quality.

This study's primary goal is to evaluate the performance metrics of the Biograph Vision 600 PET/CT system, comparing it against the benchmarks set by both the NEMA NU 2-2012 and NEMA NU 2-2018 standards [7,11]. The evaluation will encompass spatial resolution, sensitivity metrics, scatter fraction, and noise-equivalent count rate (NECR). Additionally, we will focus on the accuracy of attenuation and scatter corrections to ensure a comprehensive performance analysis.

II. OVERVIEW OF THE BIOGRAPH VISION PET/CT SYSTEM

The Biograph using an integrated 128-slice CT scanner and lutetium oxyorthosilicate PET system. It features a spacious 78 cm bore accommodating various body types as well as a sturdy table rated for loads up to 227 kg.

The PET component consists of 8 detector rings, each with 19 detector electronics modules housing two detector blocks apiece for 38 blocks total. Every block contains a grid of smaller mini blocks arranged in a 4 by 2 formation. Each mini block has a 5 by 5 matrix of 3.2 by 3.2 by 20 mm lutetium oxyorthosilicate crystals paired with a segmented 16 by 16 mm silicon photomultiplier array.

The strategic placement of mini blocks extending axially two per block results in an axial field of view of 32 mm for each block. With 8 blocks oriented lengthwise, this configuration spans a 25.6 cm axial field of view. Accounting for the spaces between blocks makes the effective axial field of view 26.1 cm.

Central to this design is a square crystal array fully covered by silicon photomultiplier detector elements. The 3.2 mm crystals ensure high spatial resolution while extensive coverage enhances light absorption, improving timing resolution and signal-to-noise ratio as studies have confirmed [13].

III. METHODS OF EVALUATION

We assessed a range of performance indicators, such as the ones listed below:

- Spatial Resolution
- Scatter Fraction, Count Losses, and Randoms Measurement
- Sensitivity
- Accuracy of Count Losses and Randoms Corrections
- Image Quality, Accuracy of Attenuation, and Scatter Corrections
- Timing resolution

The NEMA NU 2-2012 and NEMA NU 2-2018 criteria were closely followed in our assessments. The system's manufacturer provided the tools for acquisition, reconstruction, and NEMA's particular analysis. Every outcome complied with the NEMA NU 2 definitions and criteria.

A. Spatial Resolution Using F-18

Adhering to the guidelines of NEMA NU 2-2012, it's recommended to employ a point source of ^{18}F with dimensions less than 1mm in all three axes. However, given the precise features of the Vision system, a smaller point source may yield better results. Following this, the 2018 upgrade recommends the use of a ^{22}Na point source. Accordingly, a minute ^{22}Na point source was acquired from Eckert and Ziegler Isotope Products for our use. To further comply with the 2012 NEMA guidelines, an ^{18}F point source was also employed.

- Source Preparation and Positioning: A capillary tube with an inner diameter of 1mm and an outer diameter of 2 mm, containing 370 MBq/ml of ^{18}F, was utilized. A capillary tube positioning device was employed to ensure precise placement provided by Siemens Healthcare. Three-point sources were meticulously positioned at coordinates: (0, 1), (0, 10), and (0, 20) cm using the capillary tube positioning device at the center and ¼th of FOV.
- PET/CT Acquisition: A PET/CT scan was performed to accumulate at least 10,000,000 counts at the center of the axial Field of View (FOV) and at ¼th of the axial FOV from the isocenter.
- Data Collection: A back-projection technique was deployed to reconstruct the data collected from various positions after undergoing Fourier rebinning.
- Spatial Resolution Analysis: The Full Width at Half Maximum (FWHM) of each point source at various positions was determined, encapsulating radial, tangential, and axial dimensions.

The Biograph Vision demonstrated a transverse spatial resolution at FWHM of 3.7 mm at a 1 cm offset from the center of the FOV. The findings from the spatial resolution analysis at 1, 10, and 20 cm are illustrated in the succeeding Table 1.

B. Spatial Resolution Using Na-22

Thus, a 74-kBq, 0.25-mm-diameter spheric ^{22}Na point source (Eckert and Ziegler Isotope Products) was used. Acquired and processed according to the NEMA NU 2-2018 standard [2]. The results are shown in Table 1.

Table 1: Spatial Resolution Findings

Spatial Resolution:

	Distance	FWHM (mm)		FWTM (mm)	
	(cm)	Na-22	F-18	Na-22	F-18
Radial	1	3.2	3.7	6.4	7.4
	10	4.4	4.5	8.32	8.2
	20	5.7	5.6	9.9	9.4
Tangential	1	3.4	3.7	6.7	7.2
	10	3.5	3.9	6.9	8.5
	20	3.5	4	7.3	8.8
Axial	1	3.2	3.7	6.4	7.6
	10	3.5	4.3	7	9.2
	20	3.48	4.6	7.08	10.2

C. Sensitivity Analysis

Positron Emission Tomography (PET) is a pivotal imaging modality in clinical and research settings. The sensitivity of a PET scanner, defined as its ability to detect

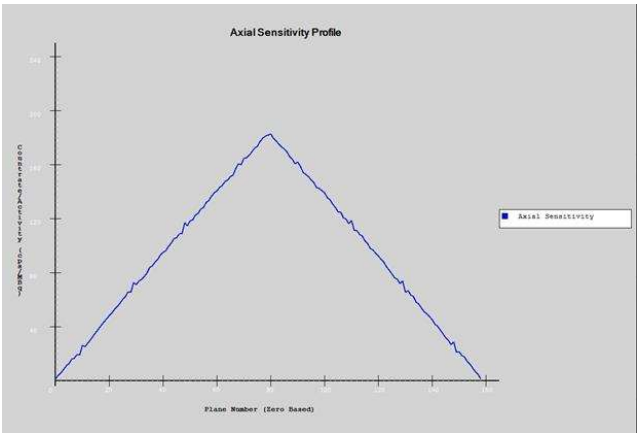

Fig 1: Axial sensitivity profiles for 0-cm off-center position

coincident photons emitted within its field of view (FOV), is a fundamental parameter affecting the quality of the imaging output. Accurate determination of scanner sensitivity is imperative for ensuring reliable and consistent imaging data. This study aims to meticulously evaluate the sensitivity of a PET scanner using a standardized NEMA PET Sensitivity Phantom.

The materials employed for this study comprised a NEMA PET Sensitivity Phantom, fillable plastic tubing of 700 mm length, (4.6 MBq) ^{18}F at the time of acquisition, various sleeves for increasing wall thickness, and low-density support materials to minimize scatter while positioning the phantom in air.

The tubing was filled with 4.6 MBq of ^{18}F and positioned centrally in the transaxial FOV with the help of low-density support materials to minimize scatter. Initially, data acquisition was performed at the isocenter. Starting with the smallest sleeve, an acquisition was carried out to collect a minimum of 10,000 true events per slice. The wall thickness was incrementally increased by adding the next smallest sleeve, with an acquisition performed at each stage, until all sleeves were utilized. Subsequently, the phantom and line sources were repositioned to a 10 cm offset from the central axis, and the acquisition procedure was reiterated for each sleeve at this offset position. The acquired data were then analyzed to ascertain the sensitivity at the isocenter and the 10 cm offset for each wall thickness, followed by an examination of the variation of sensitivity within the FOV.

The PET scanner's sensitivity was assessed at both the isocenter (0 cm offset) and a 10 cm offset from the central axis. At the isocenter, the sensitivity measured was 15.0 kcps/MBq and remained consistent at 15.0 kcps/MBq even at the 10 cm offset. The consistent sensitivity across the field of view (FOV) indicates the scanner maintains stable sensitivity critical for accurate clinical imaging data.

The vendor-stated sensitivity is 16.0 kcps/MBq, with an acceptable range of ±10% from this value. Hence, the acceptable sensitivity range is:

Lower bound: 15.0 kcps/MBq - 10% = 13.5 kcps/MBq

Upper bound: 15.0 kcps/MBq + 10% = 16.5 kcps/MBq

The measured sensitivity, although slightly below the vendor-declared value, falls within the acceptable range of 13.5 to 16.5 kcps/MBq. This confirms that the PET scanner satisfies the required sensitivity criteria. Findings are presented in Table 2 and Figure 1 and 2.

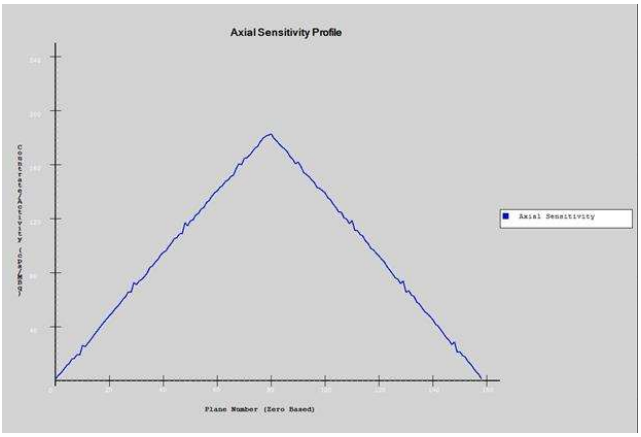

Fig 2. Axial sensitivity profiles for 10-cm off-center position.

Table 2 Sensitivity Findings

Distance (cm)	Sensitivity (kcps/MBq)
0	15
10	15

D. Scatter Fraction, Count Losses, and Randoms Measurement

The performance measurement of count rates in a Positron Emission Tomography (PET) scanner is crucial as it evaluates system count losses under various radioactivity quantities within the Field of View (FOV). Factors like scattering, count losses, and random counts significantly affect image quality and quantitation accuracy. This study employed a NEMA cylindrical polyethylene phantom and a line source of radioactivity to investigate these impacts.

The materials employed in this study included a NEMA cylindrical polyethylene phantom with a diameter of 203 mm and length of 700 mm and a line source of radioactivity containing 1.18 GBq of ^{18}F.

Multiple scans spanning over 6–7 half-lives were executed, each comprising a 15-minute scan followed by a 15-minute delay. Utilizing the PET sinogram and designated software, a meticulous analysis was conducted to evaluate true, scatter, random, and noise-equivalent count rates as a function of activity concentration.

The analysis revealed a NEMA peak Noise-Equivalent Count Rate (NECR) of 300 kcps at an activity concentration of 32 kBq/mL. Additionally, a scatter fraction of 39% was observed at the peak NECR and 37% at low activity. The vendor specification for the Peak NEC rate was also listed as 300 kcps, aligning with our findings. The results are shown in Table 3 and Figure 2.

Table 3: Scatter Fraction and Peak NECR Findings

Peak NECR (kcps at kBq/mL)	300 at 32.6
Scatter fraction (%)	
At peak NECR	39
At low activity	37

at each bed position. During scanning, coincidences along with the time of arrival were acquired and documented. A histogram depicting the differences in the time of arrival was generated from the acquired data. The timing Full Width at Half Maximum (FWHM) was then extracted from the histogram.

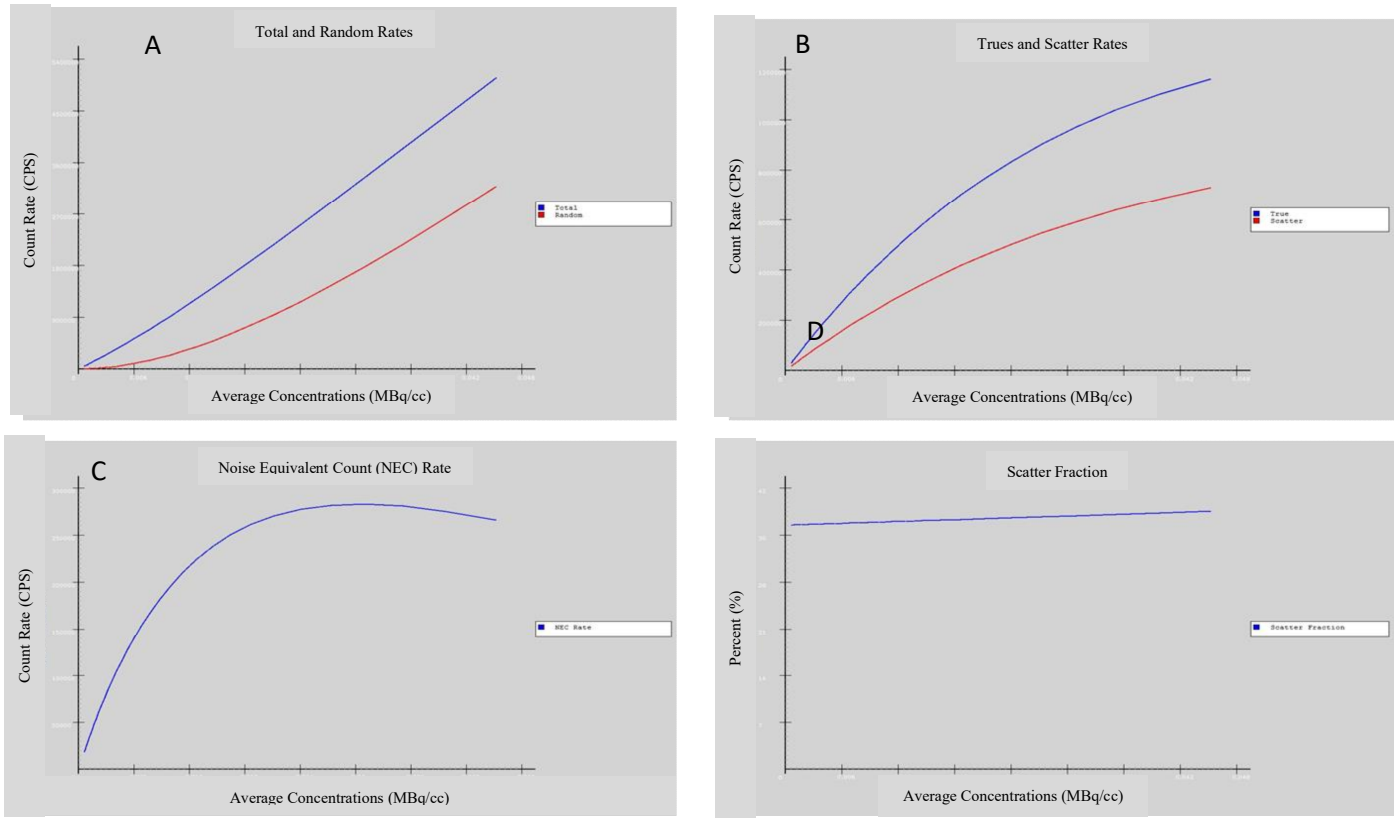

Fig 1. (A) Plots of Total and Randoms. (B) Plots of Trues and Scatter event rates. (C) Plot of NECR as a function of activity concentration. (D) The plot of Scatter fraction as a function of activity concentration.

E. Timing Resolution

Timing resolution in Time-of-Flight Positron Emission Tomography/Computed Tomography (TOF PET/CT) systems is a critical parameter as it determines the difference in the time of arrival of the two coincident photons. This difference in time is essential for obtaining information about the probable location of the annihilation event along the Line of Response (LOR). This study aims to evaluate the timing resolution of a TOF PET/CT system under varying conditions.

Line source filled with F-18 activity spanning between 27.75 MBq to 37 MBq to cover all rings. The thinnest Aluminum (Al) sleeve was used in the sensitivity test.

Initially, the line source was filled with F-18 and inserted into the thinnest Al sleeve used for the sensitivity test. A two-bed PET/CT scan was performed for 5 minutes

The evaluation yielded a detailed insight into how the TOF resolution varied with the change in count rate. The TOF resolution was observed to range from 210 to 215 and it was 213 ps as the count rate increased up to the peak NECR. This variation in TOF resolution underscores the impact of the count rate on the timing resolution of the system.

F. Image Quality Assessment

For evaluating image quality and verifying the precision of both *attenuation and scatter corrections*, we utilized the PET NEMA NU2 Image Quality (IQ) Phantom. Through gravimetric analysis, the volume of the phantom's background compartment was determined to be 9,742 mL.

The phantom also contained six spheres, each with varying internal diameters: 10 mm, 13 mm, 17 mm, 22

mm, 28 mm, and 37 mm. Central lung inserts, which was filled with polystyrene beads, remained devoid of any radioactivity.

At the onset of the image acquisition, the background activity concentration of ^{18}F stood at 5.3 kBq/mL, serving as our reference for low-activity concentration. The 4 smallest spheres were filled with a sphere-to-background ratio of 8:1 for the first set of scans and 4:1 for the second set of scans. The remaining 2 largest spheres were filled with non-radioactive water. The phantom was positioned with all spheres aligned in the axial and transaxial center of the FOV. For the simulation of a clinical situation with activity outside the FOV, the cylindric scatter phantom was placed axially next to the image quality phantom.

The line source inside the scatter phantom was filled with approximately 116 MBq of ^{18}F activity at the start of both data acquisitions. Two sequential measurements of 240 s each were acquired for a single bed position after a low-dose CT scan for attenuation correction. All data were corrected for random coincidences, normalization, decay, scatter, and attenuation. The data were reconstructed using an OP-OSEM 3D-iterative algorithm with 8 iterations and 5 subsets, applying PSF and TOF into a 440 × 440 matrix with a voxel size of 1.6 × 1.6 × 1.6 mm. The percentage contrast was obtained for hot and cold spheres, and the background count variability for each sphere was evaluated. Finally, we used the activity spillage into the non-radioactive lung insert to derive the average residual error.

The NEMA image quality phantom tests further emphasized an image contrast ranging from 77% to an impressive 92.5 % and background variability ranging from 5.2 % to 2.7 % for 4:1 and image contrast ranging from 80.79% to an impressive 90.86% background variability ranging from 3.96% to 1.43% for 8:1. The Average lung residual was 37 for 4:1 and 39% for 8:1. The results are shown in Table 4 and Table 5.

Table 4: Contrast, Background Variability, and Average Lung Residual for 8:1 Sphere-to-Background Ratio on Biograph Vision 600.

Sphere Size (mm)	Contrast (%)	Background Variability (%)
10	80.8	3.9
13	83.8	2.9
17	83.4	2.2
22	88.3	1.9
28	87.6	1.7
37	90.9	1.4
Average Lung Residual (%)	3.9	

Table 5: Contrast, Background Variability, and Average Lung Residual for 4:1 Sphere-to-Background Ratio on Biograph Vision 600.

Sphere Size (mm)	Contrast (%)	Background Variability (%)
10	77	5.2
13	85.65	4.6
17	83.1	3.9
22	86.42	3.45
28	89.4	3.1
37	92.5	2.7
Average Lung Residual (%)	3.1	

IV. DISCUSSION AND ANALYSIS

A. Spatial Resolution:

The Vision system's spatial resolution, measured in Full Width at Half Maximum (FWHM), was evaluated against the mCT Flow system using ^{18}F. The Vision system showcased transaxial spatial resolution values of 0.6 mm, 0.6 mm, and 1.2 mm at radial distances of 1 cm, 10 cm, and 20 cm, respectively. This enhancement can be attributed to the utilization of smaller 3.2-mm lutetium oxyorthosilicate crystals in the Vision system, as opposed to the 4-mm crystals in the mCT Flow system. Furthermore, the Vision system's superior axial resolution at peripheral regions might be a result of an advanced rebinning technique [12].

For precise resolution assessment, it is essential to generate a sufficiently small point source. Given that the mean positron ranges of ^{22}Na and ^{18}F are similar, any differences in spatial resolution observed are likely tied to the source dimensions [13]. Creating a small source with ^{18}F presents challenges; hence, the NEMA NU 2-2018 guidelines recommend using a ^{22}Na source for spatial resolution evaluation. Following these guidelines, our experiments incorporated a ^{22}Na point source.

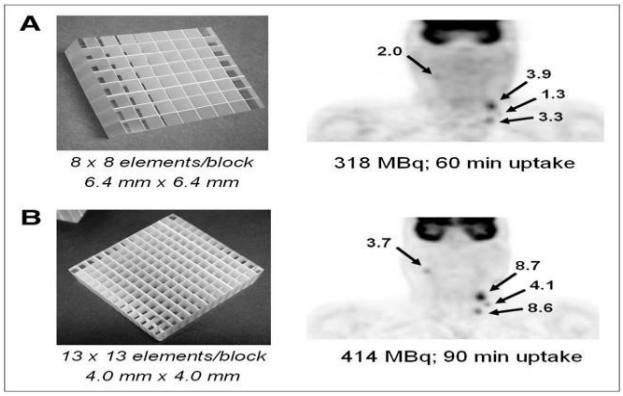

Fig.3: Comparative PET/CT scans Highlighting the Clinical Advantage of Increased Spatial Resolution in Detecting Bilateral Disease in Head and Neck Cancer. [14]

Figure 3 Comparative PET/CT scans illustrating the clinical advantage of increased spatial resolution in head and neck cancer. **(A)** The lower-resolution scan shows uptake in two left-sided lymph nodes, indicating primary disease on the left, leading to a scheduled left neck dissection. **(B)** The higher-resolution scan reveals additional uptake in a right-sided lymph node, suggesting bilateral disease. Consequently, the patient underwent a bilateral neck dissection, which confirmed the presence of disease on both sides [14].

B. Sensitivity Analysis:

The Vision 600 digital PET system has a sensitivity of 15.0 kcps/MBq, which, although slightly lower than the vendor's stated 16.0 kcps/MBq, still offers enhanced sensitivity that can significantly impact clinical PET imaging. This level of sensitivity ensures stable performance across the field of view, allowing for various benefits. These advantages include the potential for lower radiotracer doses, thereby reducing patient radiation exposure and costs, improving image quality for more precise diagnoses, decreasing scan times for patient comfort and increased efficiency, and enabling earlier disease detection. However, the deviation from the vendor's sensitivity specification underscores the necessity for ongoing performance validation in clinical settings. As shown in Figure 4. 2-D and 3-D PET images of a patient with a body mass index of 36, showing reduced noise level in the 3-D image compared to the 2-D image [15].

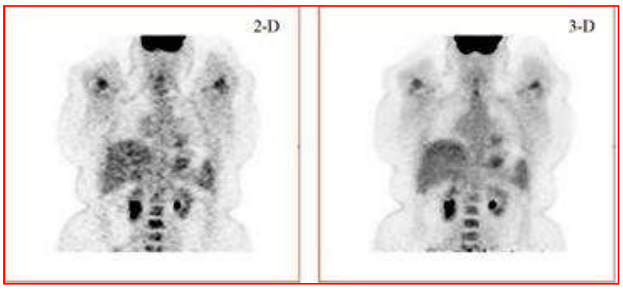

Fig 4: 2-D and 3-D PET images of a patient with a body mass index of 36, showing reduced noise level in the 3-D image compared to the 2-D image. (IAEA HUMAN HEALTH SERIES No. 27, IAEA 2014)

C. Scatter Fraction, Count Losses, and Randoms Measurement:

During the analysis of the Vision 600 digital Biograph, particular attention was given to examining the relationship between count rates and image quality, which is a pivotal aspect of PET imaging due to its direct influence on diagnostic precision.

The investigation revealed significant findings regarding the Noise-Equivalent Count Rate (NECR). At an activity concentration of 32 kBq/mL, the maximum NECR achieved was 300 kilocounts per second (kcps), aligning with the manufacturer's specified standards. NECR holds critical importance in PET imaging as it signifies the equilibrium between accurate signal detection and disruptive factors like scatter and random counts. It acts as an indicator of the system's capability to deliver high-quality images in clinical settings.

Furthermore, the study reported a scatter fraction of 37% at the peak NECR. The scatter fraction, representing the ratio of scattered gamma photons to the total count, is significant as scatter can diminish image quality by increasing background noise. A scatter fraction of this degree implies that the system can handle and maintain image clarity in the presence of substantial scatter.

The interplay between NECR and scatter fraction is crucial in determining the overall quality of images. The Vision 600's elevated NECR highlights its capacity to produce clear images even at high count rates, which is advantageous for swift scans and imaging with high activity concentration. Nevertheless, managing the scatter fraction remains vital to safeguard image sharpness and clarity.

These findings carry practical implications for clinical application. The digital PET demonstrates proficiency in managing high activity concentrations while skillfully balancing accurate and scattered counts. This competence is indispensable in clinical scenarios necessitating top-tier imaging for precise diagnosis and treatment.

D. Image Quality Evaluation

The assessment of digital PET systems (Vision 600) involved analyzing key factors such as attenuation and scatter correction accuracy, contrast, and background variability using the NEMA NU2 Image Quality (IQ) phantom. This evaluation is critical for determining the imaging performance of digital PET systems.

Tests with the NEMA IQ phantom indicated that digital PET systems could deliver high image contrast and minimal background noise. For a 4:1 contrast setting, image contrast typically fell between 77% and 92.5%, with background variability ranging from 5.2% to 2.7%. With an 8:1 contrast level, image contrast ranged from 80.79% to 90.86%, and background variability varied from 3.96% to 1.43%. These results demonstrate the capacity of digital PET systems to differentiate between areas of interest and adjacent tissue, crucial for accurate diagnosis.

Precise attenuation and scatter correction are vital in PET imaging as they ensure the accurate representation of tracer distribution in the body. Accurate correction guarantees dependable images, forming a solid basis for diagnosis. Figure 5 shows coronal whole-body FDG-PET images reconstructed with (a) and without (b) attenuation correction. The increased skin flare, hot lungs, and reduced activity in the central portion of the body in the uncorrected PET images should be noted. Figure 6 presents coronal images of whole-body FDG-PET reconstructed with (a) and without (b) scatter correction, highlighting the scatter artifacts in the uncorrected images [15].

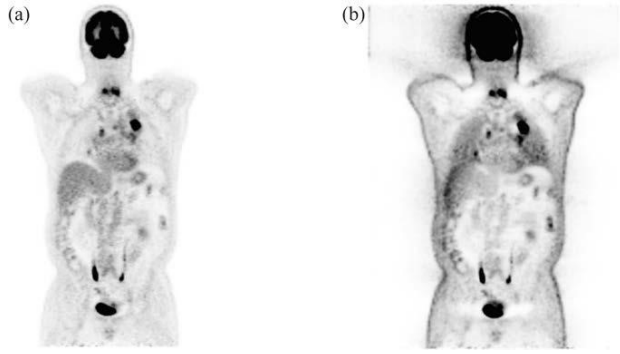

Fig.5: Coronal whole-body FDG-PET images reconstructed with (a) and without (b) attenuation correction. The increased skin flare, hot lungs, and reduced activity in the central portion of the body in the uncorrected PET images should be noted. (IAEA HUMAN HEALTH SERIES No. 27, IAEA 2014)

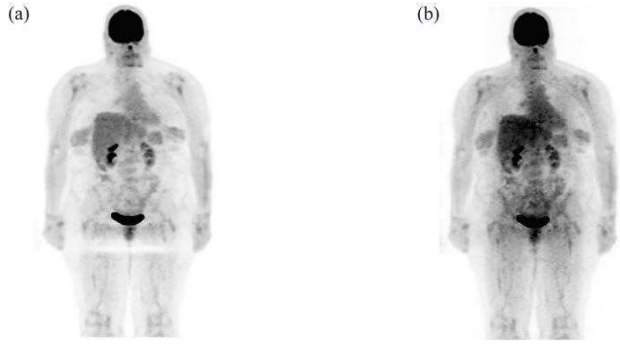

Fig. 6: Coronal images of whole body FDG-PET reconstructed with (a) and without (b) scatter correction. The scatter artifacts at the level of the hands should be noted (IAEA HUMAN HEALTH SERIES No. 27, IAEA 2014)

The research measured mean lung residual values around 37% for a 4:1 contrast ratio and 39% for an 8:1 ratio, highlighting the effectiveness of digital PET systems in visualizing regions with diverse densities, particularly in challenging lung imaging scenarios due to low density and high air content.

The implications of these outcomes are significant in clinical practice. The capability of digital PET systems to offer high contrast and low background variability is key for precise medical evaluations. Their efficiency in managing attenuation and scatter corrections further underscores their value in producing accurate diagnostic images.

E. Timing Resolution:

The assessment of the digital PET/CT (Vision 600) system primarily focused on its timing resolution, particularly the 213 picoseconds (ps) concerning Time-of-Flight (TOF) PET/CT imaging. The system's performance was evaluated against industry standards and requirements to ascertain its suitability for precise clinical diagnosis and research applications. This evaluation offers valuable insights into the capabilities of digital PET/CT systems, especially in TOF PET/CT imaging, assisting in informed decision-making for clinical purposes. Ultimately, the 213-picosecond timing resolution of the digital PET/CT system plays a critical role in determining its TOF PET/CT imaging capabilities, aiding healthcare practitioners in evaluating the system's consistency and dependability for both clinical and research uses.

V. CONCLUSION

The comprehensive assessment of the digital PET/CT system has emphasized its remarkable performance across a range of factors, including spatial resolution, sensitivity, scatter fraction, and overall image quality. The system exhibits strong adherence to established industry benchmarks and maintains uniform sensitivity throughout the entire field of view, emphasizing its reliability for both clinical and research applications. Our evaluation also highlights the importance of accounting for performance variations in different clinical scenarios. Continuous performance monitoring, quality assurance protocols, and ongoing research are vital to ensure the optimal utilization of the system in practical healthcare environments.

REFERENCES

1. Beyer T, Townsend DW, Brun T, et al. A combined PET/CT scanner for clinical oncology. J Nucl Med. 2000; 41:1369–1379.

2. Melcher CL. Scintillation crystals for PET. J Nucl Med. 2000;41:1051–1055.

3. Moses WW. Time of flight in PET revisited. IEEE Trans Nucl Sci. 2003;50:1325–1330.

4. Surti S, Kuhn A, Werner ME, Perkins AE, Kolthammer J, Karp JS. Performance of Philips Gemini TF PET/CT scanner with special consideration for its time-offlight imaging capabilities. J Nucl Med. 2007;48:471–480.

5. Jakoby BW, Bercier Y, Conti M, Casey ME, Bendriem B, Townsend DW. Physical and clinical performance of the mCT time-of-flight PET/CT scanner. Phys Med Biol. 2011;56:2375–2389.

6. Jakoby BW, Bercier Y, Watson CC, Bendriem B, Townsend DW. Performance characteristics of a new LSO PET/CT scanner with extended axial field-of-view and PSF reconstruction. IEEE Trans Nucl Sci. 2009;56:633–639.

7. National Electrical Manufacturers Association Performance Measurements of Positron Emission Tomographs. Rosslyn, VA: National Electrical Manufacturers Association; 2012. NEMA Standards Publication NU 2-2012.

8. Nguyen NC, Vercher-Conejero JL, Sattar A, et al. Image quality and diagnostic performance of a digital PET prototype in patients with oncologic diseases: initial experience and comparison with analog PET. J Nucl Med. 2015;56:1378–1385.

9. Rausch I, Ruiz A, Valverde-Pascual I, Cal-Gonzalez J, Beyer T, Carrio I. Performance evaluation of the Philips Vereos PET/CT system according to the NEMA NU2-2012 standard. J Nucl Med. October 25, 2018 [Epub ahead of print].

10. Hsu DFC, Ilan E, Peterson WT, Uribe J, Lubberink M, Levin CS. Studies of a next-generation silicon-photomultiplier–based time-of-flight PET/CT system. J Nucl Med. 2017;58:1511–1518.

11. National Electrical Manufacturers Association Performance Measurements of Positron Emission Tomographs. Rosslyn, VA: National Electrical Manufacturers Association; 2018. NEMA Standards Publication NU 2-2018.

12. Vandenberghe S, Daube-Witherspoon ME, Lewitt RM, Karp JS. Fast reconstruction of 3D time-of-flight PET data by axial rebinning and transverse mashing. Phys Med Biol. 2006;51:1603–1621.

13. Jødal L, Le Loirec C, Champion C. Positron range in PET imaging: non-conventional isotopes. Phys Med Biol. 2014; 59:7419–7434.

14. Dual-Modality Imaging: Combining Anatomy and Function David W. Townsend, Journal of Nuclear Medicine Jun 2008, 49 (6) 938-955; DOI: 10.2967/jnumed.108.051276

15. PET/CT ATLAS ON QUALITY CONTROL AND IMAGE ARTEFACTS: IAEA HUMAN HEALTH SERIES No. 27, IAEA 2014

Contacts of the corresponding author:

Author: Subhash Chand Kheruka
Institute: Sultan Qaboos Comprehensive Cancer Care and Research Center (SQCCCRC)
Street: SQU Street
City: Muscat
Country: Oman
Email: S.kheruka@gmail.com